THE JOURNAL OF BIOLOGICAL CHEMISTRY VOL. 289, NO. 35, pp. 24153–24167, August 29, 2014

Avian Facial Morphogenesis Is Regulated by c-Jun N-terminal Kinase/Planar Cell Polarity (JNK/PCP) Wingless-related (WNT) Signaling*[S]

Received for publication, September 30, 2013, and in revised form, July 3, 2014 Published, JBC Papers in Press, July 9, 2014, DOI 10.1074/jbc.M113.522003

Poongodi Geetha-Loganathan[1], **Suresh Nimmagadda, Katherine Fu, and Joy M. Richman**[2]

From the Department of Oral Health Sciences, Life Sciences Institute, Faculty of Dentistry, University of British Columbia, Vancouver, British Columbia V6T 1Z3, Canada

Background: Numerous genes contribute to the increased risk of facial clefting, but the cellular mechanisms involved are not well understood.
Results: JNK/PCP wingless-related signaling is demonstrated as a major regulator of face shape.
Conclusion: WNT11 induces clefting via inhibiting proliferation, compressing facial prominences, and changing cell behavior.
Significance: JNK/PCP WNT signaling is implicated in the pathophysiology underlying craniofacial abnormalities.

Wingless-related proteins (WNTs) regulate extension of the central axis of the vertebrate embryo (convergent extension) as well as morphogenesis of organs such as limbs and kidneys. Here, we asked whether WNT signaling directs facial morphogenesis using a targeted approach in chicken embryos. WNT11 is thought to mainly act via β-catenin-independent pathways, and little is known about its role in craniofacial development. RCAS::WNT11 retrovirus was injected into the maxillary prominence, and the majority of embryos developed notches in the upper beak or the equivalent of cleft lip. Three-dimensional morphometric analysis revealed that WNT11 prevented lengthening of the maxillary prominence, which was due in part to decreased proliferation. We next determined, using a series of luciferase reporters, that WNT11 strongly induced JNK/planar cell polarity signaling while repressing the β-catenin-mediated pathway. The activation of the JNK-ATF2 reporter was mediated by the DEP domain of Dishevelled. The impacts of altered signaling on the mesenchyme were assessed by implanted Wnt11- or Wnt3a-expressing cells (activates β-catenin pathway) into the maxillary prominence or by knocking down endogenous WNT11 with RNAi. Host cells were attracted to Wnt11 donor cells. In contrast, cells exposed to Wnt3a or the control cells did not migrate. Cells in which endogenous WNT11 was knocked down were more oriented and shorter than those exposed to exogenous WNT11. The data suggest that JNK/planar cell polarity WNT signaling operates in the face to regulate several morphogenetic events leading to lip fusion.

In craniofacial development, hox-negative cranial neural crest cells provide the majority of mesenchymal cells giving rise to the facial skeleton and connective tissue (1). Once the neural crest cells complete migration into ventral regions of the head (2, 3), buds of mesenchyme encased in epithelium, facial prominences, form around the primitive oral cavity. The facial prominences each contribute to a different region of the face as follows: the frontonasal mass gives rise to the facial midline, the maxillary prominences form the palate and sides of the upper jaw, and mandibular prominences form the lower jaw (4). The lip is formed by fusion of the frontonasal mass with the maxillary prominence, and disruption of this critical step leads to cleft lip with or without cleft palate, an all too common craniofacial defect (5).

It is thought that differential proliferation is critical for outgrowth of the facial prominences, which results in contact and eventually fusion (6–12). However, there are dramatic changes in the shape of facial prominences that may require additional mechanisms. During embryogenesis, each prominence appears to elongate in the craniocaudal axis while becoming narrower in the perpendicular or mediolateral axis. This has been documented best in the frontonasal mass (10, 13) but also takes place in the maxillary prominence (7). These shape changes are conserved in amniotes. Potential mechanisms for the rapid changes in shape may include convergent extension, directed migration, or oriented cell division. Recently, the contribution of proliferation, oriented cell division, and cellular rearrangement have been calculated in relation to the elongation of the mouse secondary palate that is derived from the maxillary prominence (14). Although proliferation still played the predominant role, up to 40% could be attributed to cell rearrangement. In an earlier study, the expansion of small groups of facial cells labeled with 1,1′-dioctadecyl-3,3,3′,3′-tetramethylindocyanine perchlorate was mapped in chicken embryos (7). Here, the authors proposed that mesenchymal cell movement was characteristic for different regions of the facial prominences. They also noted that the polarized expansion of mesenchyme was more than could be accounted for by proliferation. Using the 1,1′-dioctadecyl-3,3,3′,3′-tetramethylindocyanine perchlorate injection method, it was not possible to resolve single cells, so the ques-

* This work was supported by postdoctoral awards from Michael Smith Foundation for Health Research (to P. G.-L.), MSFHR and Canadian Institutes of Health Research (to S. N.), and Operating Grants MOP-123536 and MOP-102671 from Canadian Institutes of Health Research (to J. M. R.).
[S] This article contains supplemental Movie 1.
[1] Present address: Dept. of Biological Sciences, State University of New York at Oswego, Oswego, NY 13126.
[2] To whom correspondence may be addressed: Life Sciences Institute, University of British Columbia, 2350 Health Sciences Mall, Vancouver, British Columbia V6T 1Z3, Canada. Tel.: 604-822-3568; E-mail: richman@dentistry.ubc.ca.

tion of whether mesenchymal cells are aligned to specific axes could not be determined.

In other experimental systems, the role of individual cell polarity in maintaining tissue morphology is more defined. In epithelium, membrane and cytoplasmic proteins are distributed asymmetrically leading to apico-basal polarity that is perpendicular to the basement membrane (15). Many core components of this epithelial planar cell polarity (PCP)[3] pathway are also conserved in mesenchymal cells (16). It is not known whether facial mesenchyme cells are using PCP pathway components to orient themselves.

The PCP pathway we are studying here involves the Frizzled (Fzd) receptor that binds to WNT proteins (Wingless-related murine mammary tumor virus integration site, related to the *Drosophila* gene wingless). The disruption of the WNT PCP pathway is at the root of many embryonic defects affecting axis elongation (17, 18), endochondral bone formation (19); however, the role of this pathway in craniofacial development has not been explored in detail.

It is important to distinguish the two classes of WNTs as follows: those that are dependent on β-catenin (Ctnnb1, cadherin-associated protein β-1) and those that act independently of β-catenin. The β-catenin-dependent Wnts do not lead to recruitment or activation of PCP effector proteins. Instead, ligand binding triggers disruption of the β-catenin disruption complex, allowing shuttling of accumulated β-catenin into the nucleus where it activates transcription of target genes such as *LEF1*.

The β-catenin-independent WNTs bind to Fzd alone or receptor tyrosine kinases such as Ror2. Following binding to Fzd, the cytoplasmic protein Disheveled (Dvl) is recruited to the cell membrane. Dvl is one of the core components of the PCP pathway. After Dvl is mobilized, small GTPases, Rho and Rac, are activated, leading to JNK phosphorylation (20–22). The binding to Fzd also recruits membrane proteins Vangl2 (Van Goh-like 2) and Prickle, which are components of the PCP pathway (23). Therefore, good readouts of PCP activity include activation of JNK signaling and/or alterations in morphogenesis.

Other β-catenin-independent pathways could also be activated by WNT proteins, depending on the cellular context. The calcium pathway involves activation of protein kinase C (PKC) and calcium calmodulin kinase II (24–26). Finally, some WNTs, such as WNT5A, bind to receptor tyrosine kinase Ror2 that complexes with Vangl2 to antagonize β-catenin-mediated transcription (27). However, neither the calcium nor the Ror2-mediated pathways affect cell polarity.

A possible role for PCP-mediated Wnt signaling in human craniofacial morphogenesis is supported by the phenotypes of Robinow syndrome. Mutations in WNT5A (28) or its receptor ROR2 (29, 30) cause dominant or recessive Robinow syndrome, respectively. The phenotypes are complex and include broad nasal bridge, micrognathia, clefting, and brachydactyly. Studies on *Wnt5a* homozygous null mouse embryos suggest that altered mesenchymal cell behavior is most likely at the root of the human deformities. The shape of limb buds is altered and palatal shelves are shortened in Wnt5a mutants (31–33). However, in these mouse studies, no attempt was made to identify which type of Wnt signaling is active in craniofacial mesenchyme. One of the barriers to performing such work is that densely packed facial mesenchyme of later stage embryos is hard to image at the single cell level. Recently, the inducible confetti reporter mouse has been used to label cells and their progeny in the palate (14). This mouse model will no doubt be crossed into many mutant lines in the future. The chicken embryo face is accessible during stages of lip fusion and can be transfected with plasmids using liposomes (34). It is thus possible to combine local manipulations of signaling pathways with these transfection methods to study the effect on cell behavior.

Here, we explore the role of WNT11 in facial morphogenesis for four reasons. First, *WNT11* is locally expressed in the discrete regions of the face (35) and could be mediating facial morphogenesis. Second, WNT11 activates β-catenin-independent pathways in the majority of contexts (36), so there is a strong possibility that WNT11 will activate one or more of the these alternative WNT pathways in the face. Third, there are two animal models in which *Wnt 11* has been disrupted. Loss of *wnt11* function in *slb* (silberblick) zebrafish mutants leads to abnormal extension of axial tissues resulting in cyclopia and head defects (17). In the mouse, germ line targeting of *Wnt11* resulted in lethality at E12.0 and kidney defects in the majority of embryos (37). In this mouse knock-out, the neomycin cassette was left in the gene, which could have affected the phenotypes (38, 39). It is interesting that the transient knockdown of *Wnt11* in organ cultures of palatal shelves inhibits fusion of the palate (40). Fourth, human data suggest that WNT11 polymorphisms contribute to increased risk of facial clefting (41, 42). The animal and human data motivated us to investigate WNT11 in avian facial development.

In this study, we show that *WNT11* misexpression induces cleft lip. These effects can be attributed partly to decreased proliferation but also to abnormal morphogenesis, both of which are mediated by ectopic activation of the JNK/PCP-pathway.

EXPERIMENTAL PROCEDURES

Chicken Embryos—All animal work was approved under University of British Columbia protocol A11-0351. Fertilized chicken eggs were obtained from the University of Alberta and incubated until they reached the appropriate stage (43).

Targeting of RCAS Retrovirus to the Face—RCAS virus containing chicken *WNT11* was obtained from P. Francis-West (44) and grown in DF1 fibroblasts for 3–4 weeks as described (45). Fibroblasts expressing either RCAS::*WNT11* (44) or RCAS::*GFP* (obtained from Stephen J. Gaunt) were injected into the presumptive maxillary region of stage 15–17 embryos (46). Embryos were reincubated for 48 h, processed either for whole mount *in situ* hybridization, immunofluorescence, BrdU, or TUNEL staining as described (11, 34, 47). For skeletal analysis, embryos were incubated until stage 38 and stained for cartilage and bone as described (48).

[3] The abbreviations used are: PCP, planar cell polarity; RFP, red fluorescent protein; Fzd, Frizzled; Dvl, Disheveled; ANOVA, analysis of variance; CM, conditioned medium; DODAC, *N,N*-dioleyl-*N,N*-dimethylammonium chloride; DOPE, 1,2-dioleoylglycero-3-phosphatidylethanolamine.

Lipoplex Transfection of shRNA and RFP Plasmids in Vivo—The sh*WNT11* plasmid was obtained from others (49), and the shGFP targeting construct was cloned in our laboratory following published sequence (34, 50). Liposomes composed of 18 mM DODAC/DOPE were mixed with shRNA plasmids or empty pRFPRNAi vector to create lipoplexes. The parent vector contains a sequence coding for RFP upstream of the shRNA cassette. The lipoplex mixture was injected into the maxillary prominence at stage 18, and embryos were grown for 24–30 h until stage 23–24. Embryos were processed into wax for BrdU staining (34).

BrdU Cell Counts—The percentage of BrdU-positive cells out of the total number of DAPI-stained nuclei was counted using Northern Eclipse or ImageJ software. Three technical replicates were averaged to give the mean value for each biological replicate ($n = 3$ for all except RCAS::*WNT11*, $n = 4$). Treated and control (RCAS::*GFP,* shGFP) prominences were analyzed, and statistical analysis was carried out using Student's *t* tests with $p \leq 0.05$.

Volumetric Measurements Using the Optical Projection Tomography Scanner—Optical Projection Tomography scans (51) were carried out on embryos 48 and 72 h post-injection of RCAS::*WNT11* virus. Control embryos were not injected with virus. Following fixation in 10% formaldehyde, embryos were embedded in 1% low melting point agarose. Agarose blocks were extensively dehydrated using 4–5 changes of 100% methanol over 48 h and then were replaced with benzyl benzoate/benzyl alcohol, 2:1. Cleared and trimmed blocks were glued to mounts with cyanoacrylate and scanned on the GFP1 channel (autofluorescence, exited at 425 nm) in an Optical Projection Tomography scanner (Bioptonics, UK).

Scans were reconstructed and resliced in the frontal plane using CTAn software (version 1.10.1.0, SkyScan). A power analysis carried out on preliminary data to determine that three specimens would be sufficient to detect volume differences at 72 h following virus infection. Here, we analyzed five 48-h embryos and nine 72-h embryos injected with RCAS::*WNT11*. The volumes and dimensions of nontreated embryos were also measured (stage 24, $n = 5$, and stage 28, $n = 6$). Volumes of interest were created in Amira by tracing the maxillary prominences in individual slices. Linear measurements across the region of greatest width or height were made in rotated views. Screenshots and movies were exported for illustrative purposes. To eliminate possible stage differences between embryos, within the specimen normalization was carried out for all measurements (treated/nontreated side), and ratios were compared with nontreated control embryos of a similar stage. Ratios for 48- and 72-h specimens were analyzed using Student's *t* tests with $p \leq 0.05$.

Micromass Culture and Luciferase Assays—Embryos were injected with *WNT11* virus at stage 16, and after 48 h the infected maxillary prominences were dissected, and epithelium was removed with trypsin and dissociated as described (52). Spots of 10 μl (2×10^7 cells/ml) were plated on 35-mm Nunclon plates and allowed to attach for 1–2 h, following which 1 ml of media were added. Base media consisted of F12/DMEM 60:40, 10% FBS, antibiotic/antimycotic, L-glutamine, 10 mM β-glycerol phosphate, and 50 μg/ml ascorbic acid. Media were changed on alternate days. For a subset of experiments, cells were treated with Wnt11 or control conditioned media from the parent, and the rat B1 fibroblast cell line was transformed with empty viral vector (LNCX virus (53)). The effect of Wnt11-CM was identical to the Wnt11 virus (data not shown); to be consistent with the *in vivo* data, we used RCAS::*WNT11* for the majority of micromass culture experiments. Positive controls consisted of Wnt3a-conditioned media (activates β-catenin-mediated signaling) or Wnt5a (antagonizes β-catenin-mediated signaling and activates the JNK pathway). Conditioned media were collected the day after confluence was reached and combined 1:1 with base media.

Mesenchymal cells were transfected with various DNA constructs using DODAC/DOPE liposomes (34). Super Topflash plasmid was used to measure β-catenin-mediated Wnt activity (54) or ATF2-luc to measure PCP/JNK activity (55). *Gallus* DVL function was perturbed with mutated forms of *Xenopus* Dvl as follows: Dvl-ΔPDZ and Dvl-ΔDEP (56). In addition, the isolated *Gallus* DEP domain of DVL was cloned into pMES (gift of P. Fairlie). The lipoplex compositions were as follows: Firefly luciferase reporter (0.2 μg) + DVL plasmid (0.3 μg) + *Renilla* luciferase (0.05 μg) mixed with 0.2 μl of 18 mM DODAC/DOPE. When only Firefly reporter and *Renilla* were used, the total amount of DNA was 0.5 μg (0.375 μg of Firefly + 0.125 μg of *Renilla*). Transfection mixtures were mixed with the cell suspension just prior to plating. Relative units of luciferase activity (Firefly/*Renilla*) were detected after 48 h of cell growth using the Dual-Luciferase assay kit (Promega). For each condition, seven biological replicates were carried out. Data were normalized to LNCX control values and were analyzed by one-way analysis of variance (ANOVA), followed by Tukey's post hoc test for multiple comparisons using Statistica version 6.0. Results were considered to be significant when p was less than 0.05.

Quantitative RT-PCR—Pools of maxillary prominences were dissected and frozen in liquid nitrogen, and RNA was extracted using the RNeasy kit from Qiagen. On average five to six maxillary treated prominences were pooled into each replicate, and we collected four biological replicates for each experimental condition. SYBR-based quantitative RT-PCR was carried out in a StepOnePlus PCR machine (Applied Biosystems), using the following program: 30 s of enzyme activation at 95 °C followed by DNA denaturation at 95 °C for 5 s; annealing/extension for amplicons for 20 s at 60 °C for 40 cycles, and finally a melt curve step for 2 s at 65–95 °C in 0.5 °C increments. Human 18 S was amplified as the housekeeping control gene (ABI). Primer sequences for *Gallus WNT11, DKK1, LEF1, MSX1, MSX2, DLX5, IRF6, TBX22,* and *SOX9* were as follows: *WNT11*, forward GGCACGGGAAGTCATAAAGA and reverse GCAGAAAGGGCATACACAAATG; *DKK1,* forward GGCCCTTTGAAATCCCATCC and reverse CCTTGTTGCTACCGTCGAAG; *LEF1,* forward CATCAAGTCCTCGCTGGTC and reverse GCCCTTGTCATGGTAGGAATC; *MSX1*, forward ACAGATCCAAACGGTGAAGG and reverse AGGAGAGGAAGAGACACGG; *MSX2,* forward AGAGGCCGGGAGATATTCG and reverse TTTGGAAGGAGAAGCCATCG; *DLX5,* forward GAAGACCCAATACCTCGCC and reverse ACCCTTCTGTCAAACACTGC; *IRF6,* forward TTATGAAGTGTG-

CGATATCCCG and reverse TCTTGAATAGGGACATGCTGAG; *TBX22,* forward CGCACCTTCTCCTTCCAG and reverse GGGTTCCTATCGATCTTCAGC; *SOX9* forward CTGGGCAAGCTGTGGAG and reverse GGTTGGTACTTGTAGTCGGG.

Fold differences were calculated first relative to 18 S and then the $\Delta\Delta C_t$ method was used to calculate relative change in expression of RCAS::*WNT11*-treated RNA relative to RCAS::GFP controls or sh*WNT11* relative to shGFP controls (57). Two-tailed *t* tests were calculated on the ΔCt values for biological replicates of experimental and control samples. S.E. was calculated on the relative fold change of the biological replicates.

Cell Tracking Experiments and Confocal Microscopy, Cell Pellet Grafts—The posterior/proximal maxillary prominence was transfected with the parent pRFPRNAi plasmid that expresses RFP (50). In the same embryo, the anterior maxillary prominence was injected with Wnt11, Wnt3a, or the parent LNCX cell line (53). Cells were mixed with $DiOC_{18}(3)$ (3,3′-dioctadecyl-5,5′-di(4-sulfophenyl) oxacarbocyanine, sodium salt) to make them visible in the green channel. Embryos were incubated for 24 h, fixed in 4% paraformaldehyde, embedded in 2% agarose, and sectioned with a vibratome (75–100 μm). Sagittal sections were washed in PBS, passed through an MeOH series (25, 50, 75, and 100%) for 5 min each and then incubated in 1 μg/μl DAPI (Invitrogen) in MeOH for 30 min. Following rehydration into PBS, sections were coverslipped using Prolong Gold Antifade (Invitrogen) without DAPI. Z-stacks were obtained using a Leica TCS-SP5 confocal microscope. A long working distance 25× water immersion objective was used to increase the ability to resolve cell processes in the thick sections.

shWNT11 Knockdown in Vivo—The anterior maxillary prominence was transfected with the enhanced GFP plasmid pCAX, although the posterior maxillary prominence was transfected with the sh*WNT11* or shGFP plasmids using DODAC/DOPE. Because the native enhanced GFP signal is lost during processing, we modified the protocol to include an anti-GFP antibody step (1:2000, Synaptic System) prior to coverslipping.

Image Analysis—Confocal image stacks were imported into ImageJ. The cell counter plug-in and line tool were used. Three embryos were analyzed per treatment (two to three biological replicates and 100–200 cells per section). The proportion of total host cells labeled with RFP was located in three regions: proximal or close to the site of transfection, middle or midway between the injection site and the Wnt-secreting cells, and distal or close to the Wnt cells. The greatest distance across the cell was measured in the confocal stack using the line tool. The same cell could be tracked through several images, and a marker was placed on one end of the cell and then the other end was placed several images later. The cells were grouped into five bins as follows: bin 1, 10–15 μm; bin 2, 15–20 μm; bin 3, 20–25 μm; bin 4, 25–30 μm; bin 5, 30 μm or greater. Each bin contained five or more cells. The number of observations per bin was used for nonparametric tests. The percentage of cells out of the total number per bin was used for factorial ANOVA followed by Tukey's post hoc testing. The post hoc tests determined whether there were significant differences in cell length between the five bins and by treatment. For cell angle measurements, the image stacks were rotated to keep the position of the eye and maxillary prominence horizontal with respect to the *x* axis. This line is ~90° to the craniocaudal or vertical axis of the head. Cell angle was analyzed in 75–100 randomly selected cells taken from the image stack using ImageJ. Angular values were imported into Rose.net, Version 0.10.0.0, 2012, Todd A. Thompson Software. Data were divided into wedges or bins of 30°, and percentage observations for each bin were plotted. Polar plots were exported into Adobe Illustrator.

RESULTS

Global Misexpression of WNT11 in the Maxillary Prominence Induces Cleft Lip—During normal development of the avian face, *WNT11* is localized to the mesenchyme of the maxillary prominence and in the lateral edges of the mandibular prominence but not in the frontonasal mass (Fig. 1*A*) (35).

To begin to understand the *WNT11* function, we injected a replication-competent retrovirus RCAS::*WNT11* into the maxillary prominence at stage 15–16 (E2). Following incubation for 48 h, there was expression of exogenous *WNT11* throughout the targeted prominence with no spread to the contralateral side (Fig. 1*A*, $n = 10/10$). When allowed to grow further, the upper beak was unilaterally affected, usually displaying a notch or cleft on the treated side ($n = 14/22$, Fig. 1, *C* and *D*). In controls injected with RCAS::GFP, the embryos developed normally (Fig. 1, *E*–*E*″). Upon clearing and staining, the majority of RCAS::*WNT11*-infected embryos had skeletal defects ($n = 20/22$; Fig. 1, *C*′, *C*″, *D*′, and *D*″). Induction of clefts and bone defects are therefore the main phenotypes caused by *WNT11* misexpression in our system.

WNT11 Regulates a Subset of Genes Involved in Clefting—We next delineated the molecular pathways that could be mediating the cleft phenotypes. RCAS::*WNT11* expression was increased massively (Fig. 1*B*; 150-fold, $p = 2.00E\text{-}06$), which confirms a high titer viral infection. We examined the effect on several genes involved in the WNT pathway, orofacial clefting and intramembranous bone formation. Interestingly, of the WNT pathway genes, only the antagonist DKK1 was significantly changed (*LEF1* was not affected). DKK1 specifically antagonizes the β-catenin-dependent WNT pathway, so it is curious that there is a 60-fold down-regulation of this gene. One possibility is that WNT11 has antagonized the β-catenin-dependent pathway. The lower level of signaling may trigger the decrease in *DKK1* expression to restore homeostasis.

Clefting genes include *MSX1* (58), *TBX22,* and *IRF6* (5, 47, 58–65). Of the three, only MSX1 was decreased significantly in WNT11 gain-of-function experiments (Fig. 1*B*; *MSX1*, −2-fold, $p = 0.004$).

Because bone formation was inhibited by WNT11 retrovirus, we also examined two genes involved in intramembranous bone formation, *DLX5* (66, 67) and *MSX2* (68, 69). *DLX5* decreased by −11-fold ($p = 0.01$), but *MSX2* did not change in RCAS::*WNT11*-infected embryos (Fig. 1*B*). The decreases in *DKK1, MSX1,* and *DLX5* are the first possible targets identified for WNT11. It is likely that the down-regulation of target genes is indirect and could be mediated by changes in other signaling pathways such as the β-catenin WNT pathway.

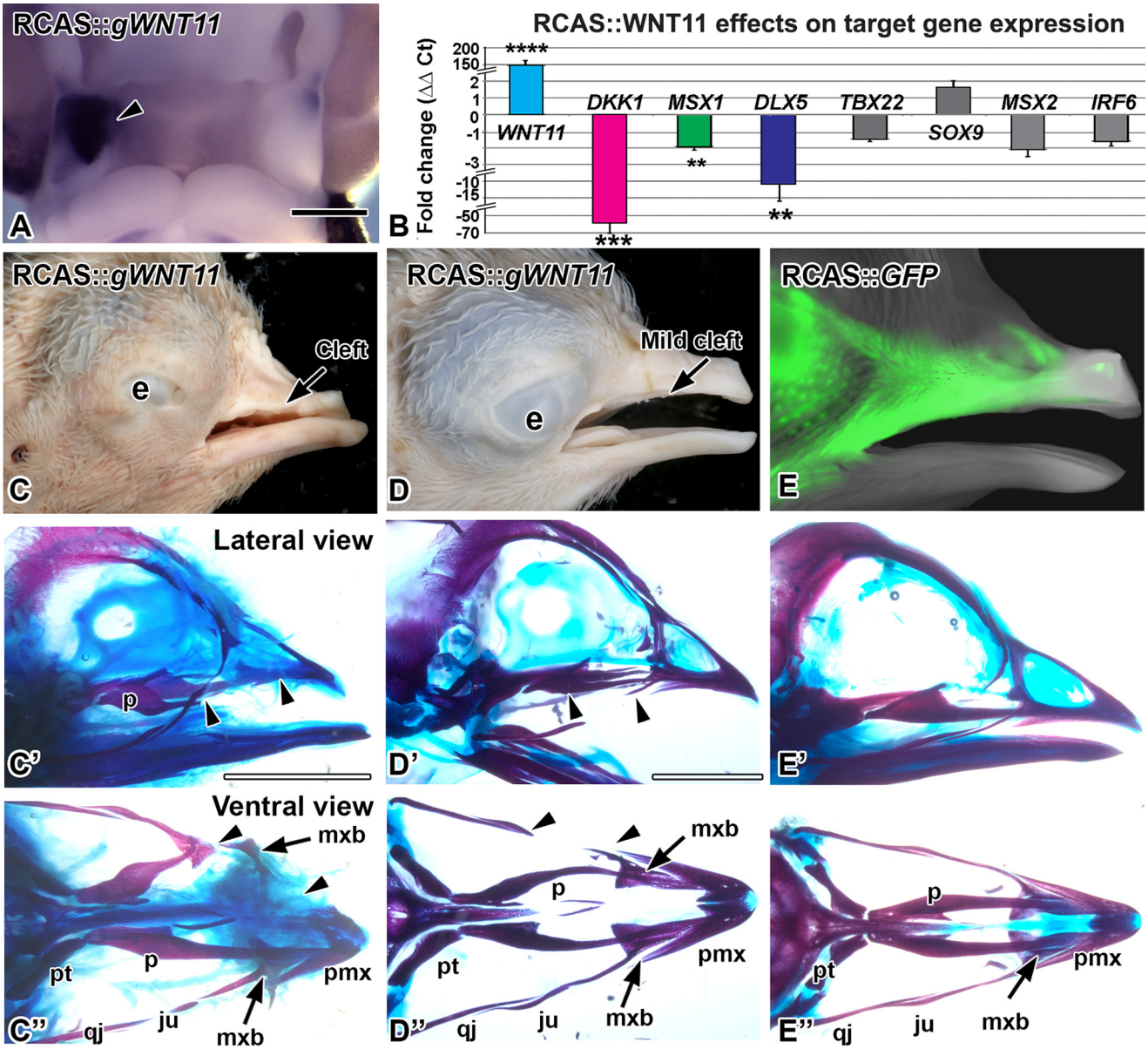

FIGURE 1. **Overexpression of *WNT11* virus causes clefts.** *A,* RCAS::*WNT11* injected into the maxillary prominence at stage 16 and fixed 48 h later at stage 24. Expression of *POL* probe confirms the virus spread on the right side (*arrowhead*). *B,* quantitative PCR measurement of gene expression change in WNT11-infected maxillary tissue, 48 h post-infection. Fold differences in expression were calculated relative to the GFP controls. *Asterisks* indicate genes that were significantly different. (****, $p < 0.00001$; ***, $p < 0.001$; **, $p < 0.01$) than GFP control RNA. *C–D″,* stage 38 embryos with RCAS::*WNT11* injected into the maxillary prominence at stage 15, photographed externally and after staining the skeleton. *C–C″,* an example of a severe phenotype with a notched upper beak or a cleft lip. The premaxilla is truncated and the palatine bone is shortened (*arrowheads*). The maxillary bone is displaced proximally (*arrow*). *D–D″,* an example of a mild phenotype with absent jugal bone (*arrowheads*). *E–E″,* a control embryo injected with RCAS::GFP at stage 15. The GFP signal is visible on the lateral side of the beak. The skeleton has developed normally. The abbreviations used are as follows: *e*, eye; *ju*, jugal bone; *mx*, maxillary prominence; *mxb*, maxillary bone; *np*, nasal pit; *p,* palatine; *qj*, quadratojugal; *pmx,* premaxilla; *pt,* pterygoid. *Scale bars, A,* 500 μm; *Bar* in *C′* applies to *C–F″*, 5 mm.

We next turned to loss-of-function experiments to tease out which aspects of morphogenesis require WNT11. No information exists on loss-of-function of *WNT11* in the head, except for the cyclopia observed in the zebrafish mutant, Silberblick (17). We used local transfection with liposomes to deliver a sh*WNT11* construct previously shown to block muscle cell elongation (49). We confirmed that this plasmid knocked down RNA expression in a previous study (34), and we measured a 10-fold knockdown with quantitative PCR (Fig. 4*F*). However, when embryos continued development, no phenotype was observed (data not shown, $n = 15$). It was possible that effects on cells were transient, and eventually gene expression was restored to normal levels. In addition, the targeting of the knockdown construct may not have covered the entire domain of WNT11 expression.

WNT11 Alters Morphogenesis of the Maxillary Prominence—It is possible that the WNT11 virus had decreased the overall volume of the maxillary prominence and/or changed a specific dimension, both of which prevented contact and fusion with the frontonasal mass. Noninjected embryos had a high degree of symmetry in their right and left maxillary prominences. Consequently, the mean ratio of right/left maxillary volumes was 0.99 (Fig. 3*F*). During the next 24 h, the maxillary prominence maintains mediolateral width while expanding in the perpen-

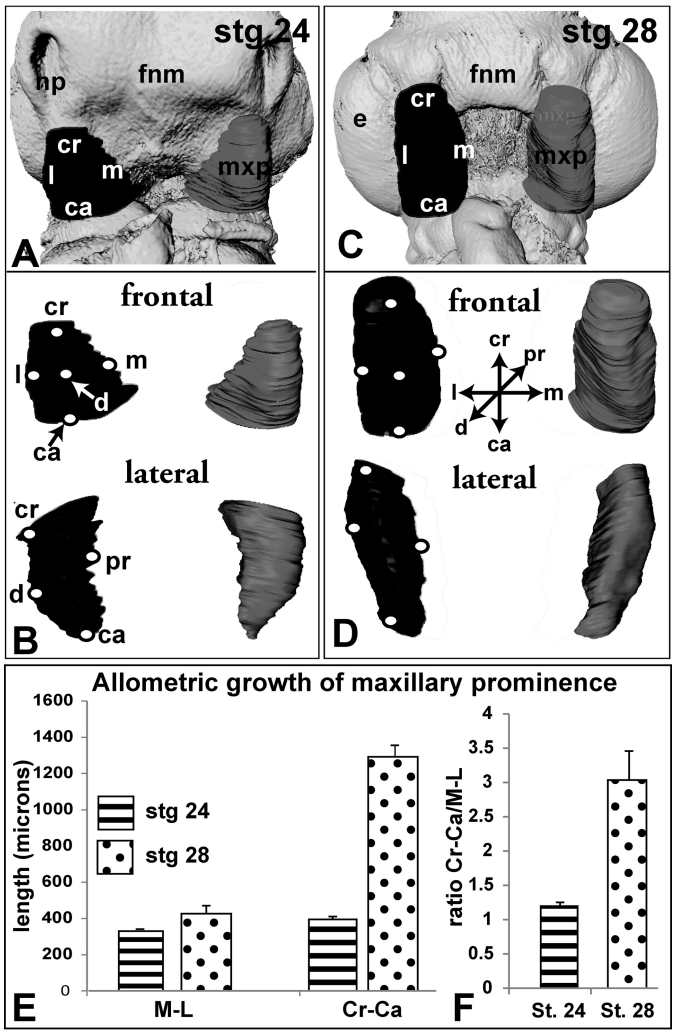

FIGURE 2. **Morphometric analysis of normal maxillary prominences between stages 24 and 28.** Reconstructed maxillary prominences at stage 24 (*A* and *B*) and stage 28 (*C* and *D*). Isosurfaces have been generated from segmented maxillary prominences using Amira. *Ridges* represent circumscribed slices. Isosurfaces are rotated to show frontal and sagittal views. *E* and *F,* at stage 24, the maxillary prominence is normally of equal size craniocaudally and medio-laterally (*Cr-Ca/ML* ratio is 1.19), whereas at stage 28, the maxillary prominence is three times as long (*Cr-Ca/ML* ratio is 3.06). The abbreviations used are as follows: *ca,* caudal; *cr,* cranial; *d,* distal; *e,* eye; *fnm,* frontonasal mass; *l,* lateral; *m,* medial; *md,* mandibular prominence; *mxp,* maxillary prominence; *np,* nasal pit; *pr,* proximal.

dicular craniocaudal axis (Fig. 2, *A–F*). The cranial-caudal length is 3-fold greater than the medio-lateral length at stage 28 (Fig. 2*F*), but at stage 24 the prominence is nearly spherical (Fig. 2*F*; cranial-caudal/medio-lateral ratio at stage 24 = 1.19 and at stage 28 = 3.06). The allometric growth of the maxillary prominence is striking and may indicate that convergent-extension morphogenesis is taking place.

The volume of the *WNT11*-treated maxillary prominence was not significantly different from noninjected controls at 48 h (Fig. 3*F*, $p = 0.3894$); however, at 72 h the treated prominences were significantly smaller (Fig. 3, *A–E*, $p = 0.0005$, supplemental movie 1). The virus does not spread to the contralateral side of the face within such a short period of embryonic growth as shown by the similar dimensions in nontreated controls and contralateral maxillary prominences (Fig. 1*A*). Quantification revealed that not only was the absolute cranial-caudal length shorter (Fig. 3*G*; 968 ± 45 μm for control and 829 ± 57 μm for treated, $p = 1.6E-05$) but so was the mean proximo-distal length (Fig. 3*G*; 485 ± 45 μm for control and 405 ± 24 μm for treated, $p = 0.0001$). The medio-lateral width was unchanged (Fig. 3*G*; 394 ± 21 μm for control and 375 ± 32 μm for treated, $p = 0.0790$). The ratio of cranial-caudal length over ML length was significantly reduced in *WNT11* treated maxillary prominence when compared with noninjected controls (Fig. 3*H*; $p = 1.43E-05$). These maxillary shape changes could contribute to a failure of contact with the frontonasal mass, thus leading to cleft lip.

WNT11 Negatively Regulates Proliferation—The volumetric and shape distortions caused by RCAS::*WNT11* suggested that cellular dynamics were altered. Indeed, proliferation was significantly reduced in RCAS::*WNT11*-infected mesenchyme (Fig. 4, *A*, *A″*, and *E*; $p = 0.0002$, $n = 4$) compared with the control RCAS::*GFP* embryos (Fig. 4, *B–B″*, and *E*; $n = 3$). Typical patterns of proliferation are observed on the unoperated side (Fig. 4*A′*). There was no increase in apoptosis ($n = 3$, data not shown) excluding this as a mechanism for the clefting.

To determine the normal role of WNT11 in regulating proliferation, we analyzed embryos transfected with the knockdown sh*WNT11* plasmid. A significant increase in proliferation occurred (Fig. 4, *C–C″* and *E*; $n = 3$; $p = 0.002$), although the control sh*GFP* plasmid had no effect (Fig. 4, *D–D″,* and *E*; $n = 3$). Thus, even though sh*WNT11* did not lead to skeletal defects, the significant increase in proliferation observed at 24 h indicates that the normal role of WNT11 is to repress proliferation.

The fact that the sh*WNT11* plasmid had effects on proliferation 24 h post-transfection suggested that other molecular changes may have been induced. Indeed, we found that several genes were differentially expressed, including *DKK1, LEF1*, *MSX2*, and *SOX9* (Fig. 4*F*). *SOX9*, *MSX2,* and *LEF1* were not affected in response to the virus but were decreased 8-, 5-, and 4-fold, respectively, in the shRNA knockdown. Thus, these genes require WNT11 to maintain their expression, but WNT11 was not sufficient to up-regulate their expression. Interestingly, in the case of *DKK1,* we did see a 2-fold up-regulation, which is in opposition to the significant decrease induced by overexpression of WNT11 (compare Figs. 1*B* to 4*F*). These results support the concept that by lowering WNT11, the β-catenin-dependent pathway is more active, and therefore *DKK1* is raised to restore equilibrium. However, the 4-fold reduction in *LEF1* after sh*WNT11* overexpression suggests that there is less, rather than more, β-catenin available. Further biochemical assays are needed to unambiguously determine the effect of WNT11 on the β-catenin-dependent pathway.

WNT11 Antagonizes Super Topflash Reporter Activity—To investigate in more detail the signaling effects of WNT11 within facial mesenchyme, we took advantage of sensitive WNT reporter assays that indicate activity of either the β-catenin or the JNK pathway (Super Topflash or ATF2 reporters, respectively). To maintain the context, the reporters were transfected into high density micromass cultures of maxillary mesenchyme (52, 70). We continued to use the same *WNT11* retrovirus as in the *in vivo* experiments so as to mimic as closely as possible the conditions present in the whole embryo (Fig. 5, *A–G*). We also did a comparison experiment in which condi-

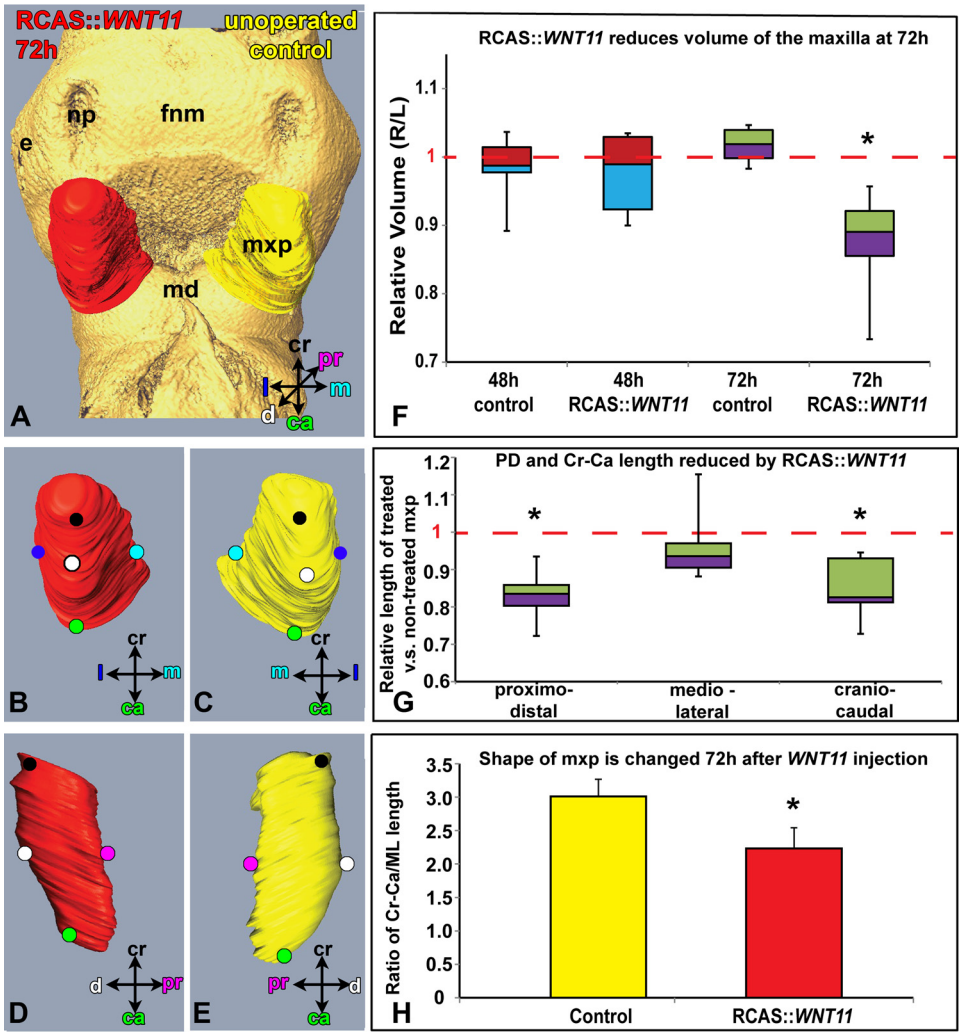

FIGURE 3. **Morphometric analysis of *WNT11*-infected and control maxillary prominences.** *A,* reconstructed maxillary prominences 72 h post-infection with RCAS::*WNT11*. Isosurfaces are rotated to show frontal (*A–C*) and sagittal views (*D* and *E*) of treated and left side, control maxillary prominences. *F* and *G,* box plot where *boxes* represent the mean of five to six biological replicates for each of the controls and five to nine replicates for the WNT11-infected embryos. The *top* and *bottom* of the boxes represent the 25th to 75th quartile, and *error bars* represent the minimum and maximum values. *F,* control embryos have very little right-left variation in volume (mean value is close to 1, *dashed line*). The mean ratio 48 h post-infection is not significantly different from 1, indicating the virus has no effect at this time. In contrast, 72 h post-infection the ratio of treated/untreated maxillary volume is significantly less than 1 ($p < 0.05$). *G,* majority of change in volume at 72 h is due to decreased proximo-distal and cranial-caudal length. *H,* ratio of craniocaudal length over medio-lateral length is significantly reduced in RCAS::WNT11-treated maxillary prominence when compared with controls ($p = 1.43E-05$). The abbreviations used are as follows: *ca,* caudal; *cr,* cranial; *d,* distal; *e,* eye; *fnm,* frontonasal mass; *l,* lateral; *m,* medial; *md,* mandibular prominence; *mxp,* maxillary prominence; *np,* nasal pit; *pr,* proximal.

tioned media from a cell line that stably expresses mouse Wnt11 (82) was added to the maxillary cells once they were place in culture (data not shown).

The Super Topflash reporter was strongly induced in response to the positive controls (Wnt3a-conditioned media and LiCl, an antagonist of GSK3β that is a part of the β-catenin destruction complex; Fig. 5*A*). These data confirm that the maxillary mesenchyme has the necessary signal transduction machinery to respond appropriately to increase β-catenin signaling. However, *WNT11* is a potent antagonist of β-catenin signaling when activated by Wnt3a (Fig. 5*A*). *WNT11* is unable to antagonize the activation of the reporter when LiCl is added (Fig. 5*A*). This is different from our previous study where WNT5A was able to antagonize Wnt3a and LiCl in similar culture conditions (70). The antagonistic effects of *WNT11* are therefore dependent on GSK3β. We next used the sh*WNT11* plasmid and found the reduction of *WNT11* resulted in a striking activation of the Super Topflash reporter (Fig. 5*A*). These data are consistent with the increase in *DKK1* expression described earlier. Therefore, during normal development WNT11 is likely to be antagonizing β-catenin-dependent pathways in areas of the face where it is highly expressed.

The intracellular mediator DVL is involved in transducing all WNT pathways that act via FZD receptors. The specificity lies in which domain of DVL, the DIX, PDZ, or DEP domains, is mediating the signal transduction. The DIX and PDZ domains are used in both β-catenin-dependent and -independent signaling, whereas the C-terminal DEP domain directs activity entirely toward the PCP/JNK signaling pathway (71). The functional consequences of deleting the DEP domain in chicken embryos are to block cell reorganization during gastrulation and myotome formation (49, 56, 72). No one has studied the role of the DVL domains in primary cell cultures. Here, we confirmed that the PDZ domain is required for Super Topflash

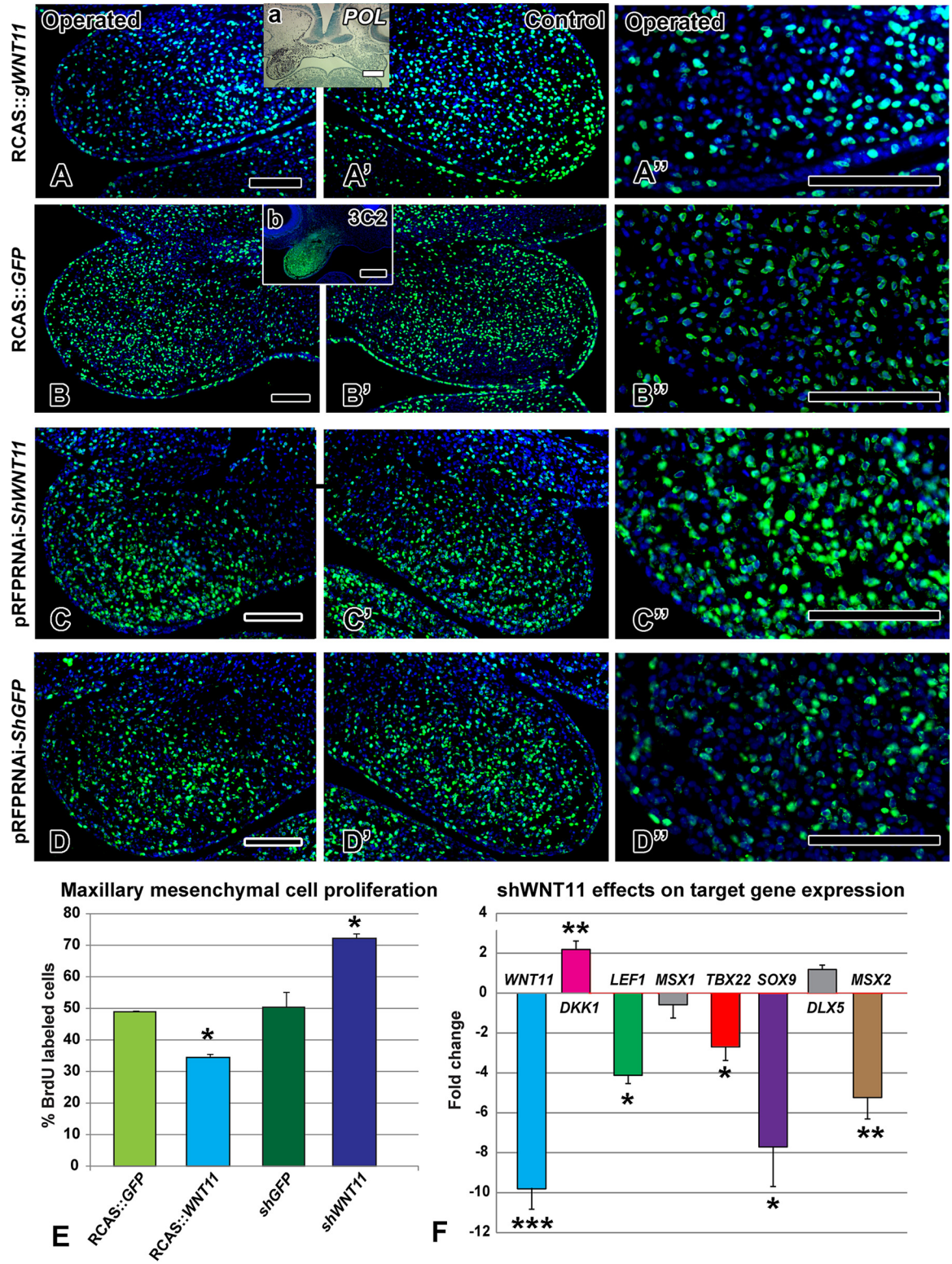

FIGURE 4. **WNT11 regulates cell proliferation and gene expression.** BrdU antibody staining 48 h after viral infection or 24 h post-transfection with shWNT11 plasmid. *Insets* are adjacent sections to show location of the virus with a *pol in situ* probe (*a*) or an antibody to viral Gag protein (*b*). *A–A″* and *E,* decreased proliferation is seen in the *RCAS::WNT11* treated maxillary prominence ($p = 0.001$). *B–B″* and *E,* normal proliferation is observed in the *RCAS::GFP*-infected embryos compared with the control, contralateral side. *C–C″* and *E,* local transfection with a sh*WNT11* plasmid at stage 18 increased proliferation at 24 h ($p = 0.0001$). *D–D″* and *E,* control sh*GFP* plasmid levels were indistinguishable from the RCAS::GFP embryos. *F,* fold-change in expression levels of genes measured 24 h post-transfection with shWNT11 plasmid. ***, $p < 0.001$; **, $p < 0.01$; *, $p < 0.05$. *Scale bars,* 100 μm.

activity (Fig. 5*B*) when Wnt3a is added. However, the DEP domain is neither sufficient nor required for β-catenin-mediated activity (Fig. 5, *C* and *D*) as shown for other cell types.

WNT11 Activates JNK Activity in Facial Mesenchyme via the DEP Domain of DVL—We hypothesized, based on the morphogenesis changes, that WNT11 had activated PCP-type signaling

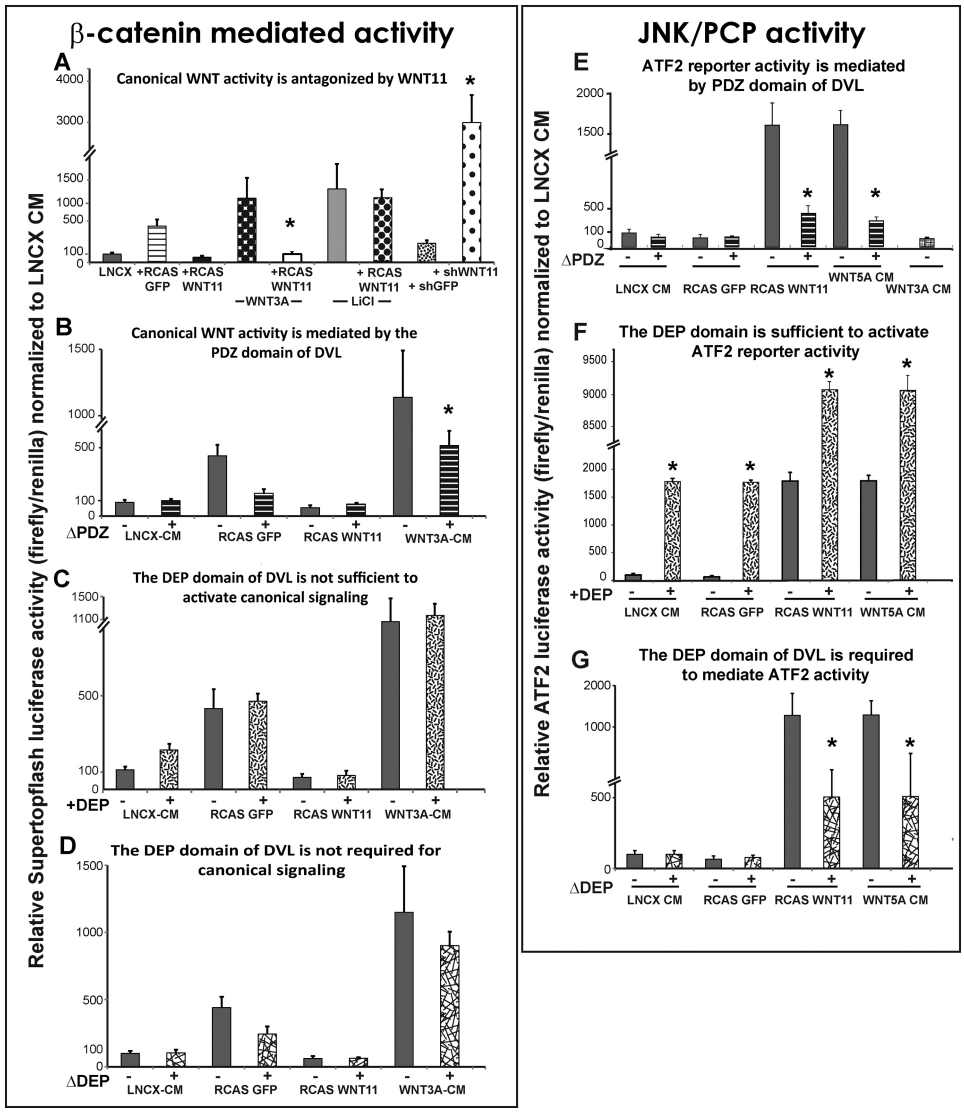

FIGURE 5. **Reporter quantification of WNT activity in maxillary mesenchyme.** Data are represented as means of seven replicates and *error bars* = 1 S.D. All data were normalized to LNCX values. Data comparisons between conditions were made using ANOVA followed by Tukey's post hoc testing. Wnt3a, Wnt5a, and LNCX were added as conditioned media. *GFP* and *WNT11* treatments involved pre-infecting maxillary mesenchyme with the relevant viruses at stage 16 followed by isolation of the virus-infected mesenchyme from stage 24 embryos. Plasmids containing sh*WNT11*, sh*GFP*, the luciferase reporters, or the *DVL* variants were transfected at the time of plating. *A,* exogenous *WNT11* blocked activation of Super Topflash by Wnt3a-conditioned media but not by LiCl. Knockdown with sh*WNT11* derepressed the endogenous gene and activated the reporter. *B,* DVL-ΔPDZ reduced Super Topflash activity induced by Wnt3a-CM as expected. *C,* DEP domain fails to activate the reporter. *D,* removal of the DEP domain has no effect on β-catenin-mediated activity. *E, WNT11* and Wnt5a activated the ATF2 reporter by 15-fold relative to the controls. The addition of DVL-ΔPDZ blocked the activation of the ATF2-reporter by *WNT11* and Wnt5a. *F,* isolated DEP domain is sufficient on its own to activate ATF2 to similar levels produced by *WNT11* or Wnt5a-CM. The DEP domain combined with *WNT11* or Wnt5a-CM results in a massive synergistic effect on the level of ATF2 luciferase activity. *G,* DVL-ΔDEP dampens activation of the ATF2-luc reporter by *WNT11* virus or Wnt5a-CM.

and that DVL was mediating this activity. We used an ATF2 luciferase reporter, which is a robust readout for JNK signaling in *Xenopus* embryos (55).

We determined that the *WNT11* virus strongly activates the ATF2 reporter as does the positive control, Wnt5a-conditioned media (CM) (Fig. 5*E*). Wnt3a-CM fails to activate the reporter (Fig. 5*E*). The deletion of both the PDZ (Fig. 5*E*) and DEP (Fig. 5*F*) domains significantly blocks activation of the ATF2-luc reporter by *WNT11* virus. Addition of the isolated DEP domain increased basal ATF2 activity above controls (Fig. 5*F*); however, when added to cultures infected with RCAS::*WNT11,* there was a remarkable synergistic effect (Fig. 5*G*). These data strengthen the link between *WNT11* and β-catenin-independent signaling. Moreover, the specific involvement of the DEP domain confirms that PCP pathways are involved in transducing the signal.

Wnt11 Acts as a Chemo-attractant in the Face—Based on the changes in morphology of the maxillary prominence and the activation of PCP-type signaling, there was justification to explore in more detail the role of WNT11 on the individual cell morphology that is often affected when JNK/PCP signaling is perturbed. Furthermore, cell behavior analysis could be used to determine which signaling pathway is most active in gain- and loss-of-function experiments *in vivo*. Focal transfections of host mesenchyme with an RFP plasmid were combined with cell injections into the opposite end of the maxillary prominence. The identical cell lines used to express conditioned

media for luciferase assays were used for these experiments (Wnt11, Wnt3a, or LNCX parent cell lines for the stably transformed Wnt cell lines). Slightly older embryos (stage 24) were injected to allow a sufficient separation between the host and source cells (~350 μm), and embryos were followed for 24 h. In the presence of Wnt11, many RFP-labeled cells passed the level of the choroid fissure of the eye (3/3) and intermingled with the donor Wnt11 cells (Fig. 6*A*′). However, in embryos injected with Wnt3a, cells reached the choroid fissure but did not intermingle with the donor cell pellets (Fig. 6, *B* and *B*, 3/3). Similarly, control LNCX cells do not induce movement of RFP-positive host cells past the choroid fissure (Fig. 6, *C* and *C*′, 3/3). In both Wnt3a- and LNCX-treated embryos, the RFP-positive cells expanded into a streak beneath the eye. The proximodistal expansion therefore represents the normal pattern of growth in this region of the maxillary prominence.

We quantified the spread of host mesenchymal cells by counting the proportion of labeled cells in thirds of the maxillary prominence, close to the transfection site (proximal), midway (center), and close to the donor cells (distal). We found that in Wnt11-treated embryos ($n = 3$), 40% of cells were in the proximal third, 45% were in the middle third, and 25% were found in the distal third of the maxillary prominence close to the donor cells (Fig. 6*D*). In Wnt3a ($n = 2$) or LNCX-treated embryos ($n = 2$), 75% of cells were in the proximal third, and the remaining 25% was divided between the middle and distal thirds (Fig. 6*D*). We confirmed that there was no decrease in the size of the maxillary prominence during the 24-h experimental period (Fig. 3*F*). Therefore, the movement of cells toward the source of Wnt11 was not due to contraction of tissues, bringing together the site of injection and the site of cell implantation.

Because PCP signaling affects the cytoskeleton, we analyzed several parameters relating to cell morphology. The typical maxillary mesenchyme cell is ~10–20 μm in length and is characterized by numerous cell processes extending in all directions. Measurements of the length of the major axis revealed that the type of cell pellet had no effect on length (factorial ANOVA, data not shown). We also examined the orientation of cells relative to a horizontal line connecting the anterior margin of the maxillary prominence and the eye. The data suggest that although there is generally a high degree of orientation in mesenchymal cells, there is slightly more variability in orientation of the Wnt11-exposed cells (Fig. 6, *E*–*G*). The migration and randomized cell orientation effects combined with the luciferase data support the idea that WNT11 is capable of activating a subset of PCP-type mechanisms in the face.

WNT Knockdown Leads to Shorter, More Oriented Cells—The data thus far have shown that exogenous *WNT11* is capable of activating PCP/JNK signaling and is sufficient to alter cell behavior. However, we wanted to address whether WNT11 is required for orientation, cell movement, and elongation of mesenchymal cells. We used the sh*WNT11* construct that also expresses RFP and transfected this plasmid into the posterior maxillary prominence (Fig. 7, *A*–*B*‴). The GFP plasmid, pCAX, was transfected anteriorly to detect long range effects of knocking down WNT11 (Fig. 7, *A*‴ and *B*‴). There were no differences in cell length or orientation of the anterior pCAX-labeled cells suggesting that either there was no long range signaling or that, for technical reasons, knockdown was insufficient to produce a phenotype. There was also no qualitative change in the distribution of RFP or GFP cells in macroscopic examination of experimental and control specimens ($n = 12$ for control shGFP and $n = 12$ for shWNT11). In contrast, there were significant cell-autonomous effects observed with confocal analysis. Cells expressing sh*WNT11* ($n = 3$) were shorter than control shGFP cells ($n = 4$, Kolmogorov-Smirnov test, median significantly different, $p < 0.001$, Fig. 7, *C* and *D*). In addition, factorial ANOVA revealed that the percentage of shWNT11 cells in Bins 4 and 5 was lower compared with shGFP ($p < 0.001$). Finally, the angle of sh*WNT11* cells appeared to be less random than shGFP cells (Fig. 7, *E* and *F*). Thus, lowering the level of WNT11 may allow the cells to align themselves to other morphogen gradients.

DISCUSSION

Here, we determined that WNT11 acts through pathways independent of β-catenin to regulate several key aspects of facial morphogenesis, including the elongation of facial prominences, proliferation, lip fusion, and skeletal patterning (Fig. 8). At the molecular level in primary cultures of facial mesenchyme, we determined Wnt11 but not Wnt3a is sufficient to activate the JNK/PCP pathway via the DEP domain of DVL. We also demonstrated cross-talk with the β-catenin-dependent WNT signaling pathway such that antagonism requires an intact GSK3β complex. At the cellular level, we demonstrated that endogenous WNT11 is required for cells to elongate and proliferate. WNT11 is also sufficient to act as a chemo-attractant in the face and to randomize cell orientation.

WNT11 Affects Processes Involved in Lip Fusion—Formation of the primary palate or lip involves outgrowth of adjacent facial processes, contact between epithelia, followed by degradation of the epithelial seam and formation of a mesenchymal bridge. This process is largely conserved in humans (73, 74), mice (75, 76), and chickens (11, 77). Much of our previous work had focused on two mechanisms, decreased proliferation and increased apoptosis inhibited lateral outgrowth and contact of the facial prominences (11, 77). Here, we showed that initially at stage 24 there was a decrease in proliferation; however, the volume and shape of the maxillary prominence were unaffected. In the next 24 h (72 h post-infection), the shape changes became apparent (15% decrease in craniocaudal and proximodistal length). The timing of proliferation and shape changes suggests they are related and lead to clefting. It is logical that impacting the axis in which the most growth occurs leads to clefting.

In normal development, the absolute width of the maxillary prominence is increased by 20% between stages 24 and 28. In contrast, the craniocaudal length is increased by 300%. In a previous study, we mapped proliferation in different regions of the normal maxillary prominence across stages 24–29 (78). We found that at stage 24, the proliferation was even throughout the mesenchyme, but at stage 28, more proliferating cells were found in the caudal mesenchyme. By stage 29, this trend was reversed, and relatively higher proliferation was seen cranially. The specific pattern of proliferation at stage 28 could account for some of the dramatic lengthening of the maxillary promi-

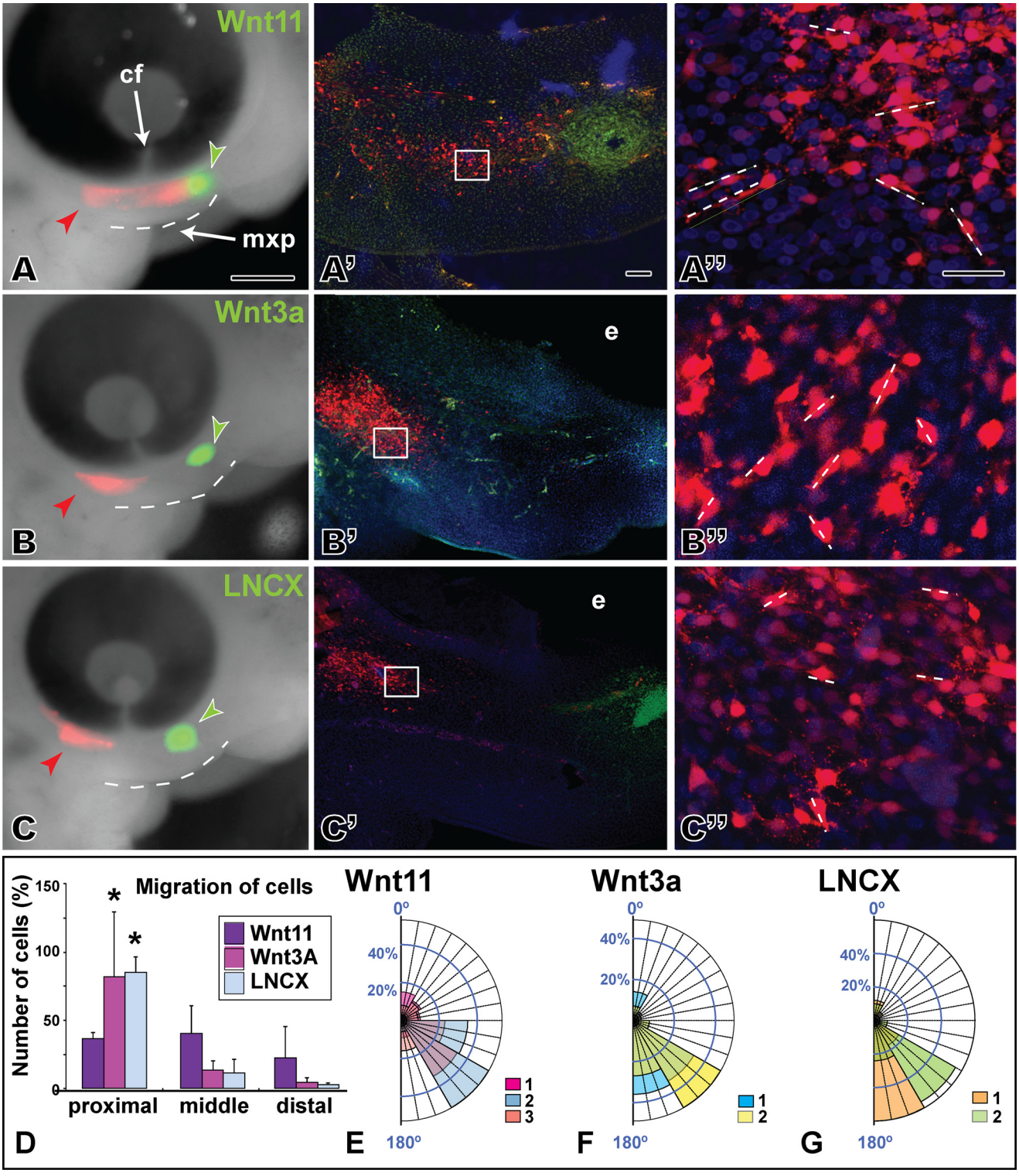

FIGURE 6. **Chemotaxis is induced by Wnt11 cells but not by Wnt3a or the control.** *A, left column* is view of embryos 24 h after injection of Wnt-secreting cells (*green fluorescence*) and transfecting host mesenchyme with an RFP expression plasmid (*red fluorescence*). The maxillary prominence is outlined with a *dashed line*. *Middle* and *right columns* are sagittal vibratome sections through the same embryo in which native RFP fluorescence is visible. *Middle column* is maximum intensity projections of a confocal stack through ~75 μm of tissue. The *right column* is a higher power maximum projection through ~20 μm of tissue. *Short dashed lines* show greatest extension of filopodia and major axis of a particular cell. *A–A″*, host cells have spread past the choroid fissure and seem to be migrating toward the pellet of Wnt11-expressing cells. Confocal images from halfway between the injection point and the cell pellet. *B–B″*, host cells have expanded but not passed the choroid fissure. *C* and *C′*, normal patterns of cell movement/expansion are seen in the controls. *D, bars* represent the average cell number from two to three biological replicates plus 1 S.D. Host cells in Wnt11-treated embryos are found in proximal, middle, and distal zones, whereas for Wnt3a or LNCX control embryos the majority of cells are proximal. *E–G*, angular data from host cells exposed to different types of cell pellets. Data are arranged as percentage observations for each 30° segment. Each color represents data from different embryos, and where data overlaps, the colors are combined. *E*, Wnt11 appears to have slightly more random cell orientation than Wnt3a (*F*) or LNCX (*G*) cells. The abbreviations used are as follows: *cf*, choroid fissure; *mxp*, maxillary prominence. *Scale bar*, 500 μm for *A–C*, 50 μm for *A′–C′*, and 25 μm for *A″–C″*.

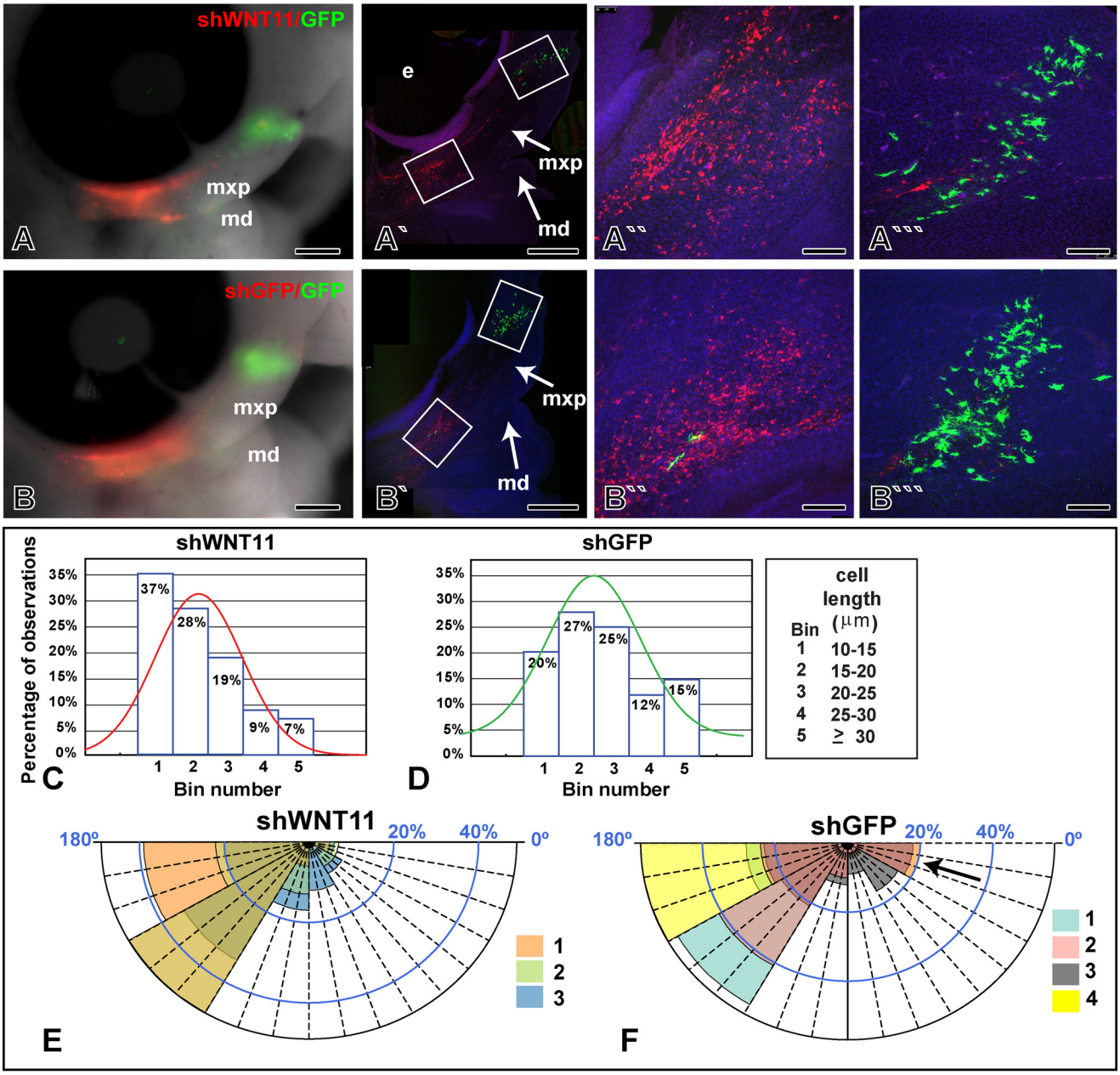

FIGURE 7. **Knockdown with shWNT11 plasmid shortens and orients cells.** *A* and *B*, macroscopic views of embryos transfected with RFP-shWNT11 or the control, RFP-shGFP plasmids posteriorly and GFP plasmid anteriorly. Transfections were carried out at stage 18, and embryos were grown for 24 h until they reached stage 24. *A′–B‴*, confocal images of sagittal slices through the face. The transfection of the RFP plasmid was increased relative to Fig. 6 to more effectively knock down *WNT11* expression. Red cells reflect native RFP signal, and green cells were stained with an anti-GFP antibody. More of the cell processes are visible in the antibody-stained cells giving the impression they are larger than the RFP cells. *C* and *D*, histograms showing distribution of cells according to length measurements taken in Image J, across the stack. Only RFP-positive cells are shown. The *curves* show the general distribution of observations about the median. The shGFP cell curve is shifted toward higher bin numbers than the shWNT11 curve. *E*, close clustering of cell orientation wedges in shWNT11-transfected cells. *F*, more randomized orientation of shGFP cells (*arrow*) in an equivalent region of the maxillary prominence. Each color represents data from a different embryo. The abbreviations used are as follows: *md*, mandibular prominence; *mxp*, maxillary prominence. *Scale bar*, 500 μm for *A*, *A′*, *B*, and *B′*, 100 μm for *A″*, *A‴*, *B″*, and *B‴*.

nence, especially because in the perpendicular medio-lateral axis, there is relatively even proliferation. In the presence of the WNT11 virus, the patterns of proliferation were disrupted, and this prevented elongation of the prominence in the cranial-caudal axis.

Linking together the data on shape changes with the cellular data, it is likely that the virus has randomized the orientation of cells all over the maxillary prominence, and this contributed to the decreased craniocaudal and proximo-distal growth. The WNT11 knockdown data where cells were more highly aligned raise the possibility that another unidentified signal is taking on the role of orienting cells in the craniocaudal axis. A candidate could be the fibroblast growth factor (FGF). When the FGF pathway was activated with RCAS viruses, a downstream negative feedback loop was induced (79). The net effect was a decrease in pathway activity. Cells in the frontonasal mass became randomized. Because *FGF8* is expressed asymmetrically in the maxillary

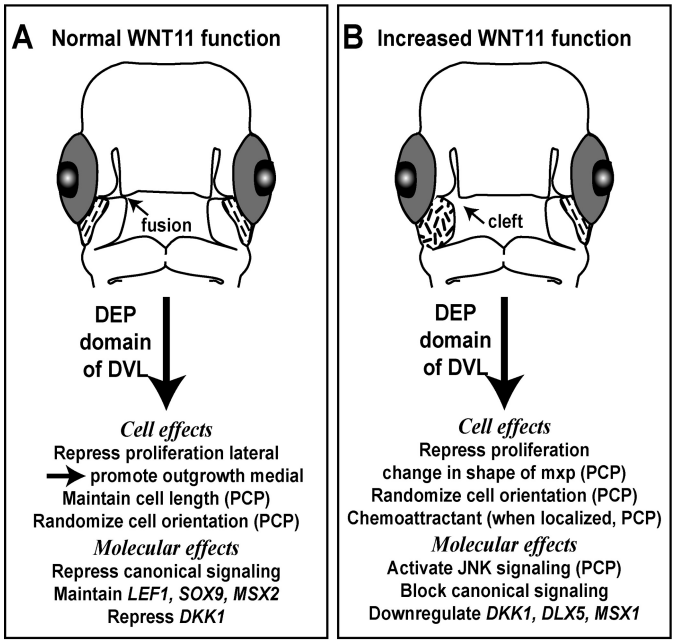

FIGURE 8. **Roles of WNT11 during facial morphogenesis.** *A,* during normal morphogenesis, WNT11 is expressed at the lateral or proximal edges of the maxillary prominence under the eye (*dashed lines*). Data from sh*WNT11* knockdown revealed multiple roles on cell behavior and molecular signaling, some of which are characteristic of PCP pathways in other cell types (*PCP*). *B, WNT11* overexpression in the right maxillary prominence (*short dashes*) is sufficient to induce clefts. The mechanisms include several processes that are typical of PCP signaling in other cell types.

prominence (11), FGF is a long range signal (80) that could be utilized to orient cells.

Cell-autonomous Roles for WNT11—The approach of using the shWNT11 plasmid has revealed three new cell-autonomous roles for WNT11. These include the following: regulating proliferation, cell length, and cell orientation. Cell proliferation is normally repressed by WNT11. Indeed, there is a good correlation between the area of high *WNT11* expression under the eye (35) with the relatively lower proliferation index (78). The function of WNT11 may be to create the gradient of proliferation in the maxillar prominence that is necessary to promote contact and fusion with the frontonasal mass.

The decrease in cell length supports the idea that cells require WNT11 to form filopodia. We showed that cells were more oriented when expressing the sh*WNT11* plasmid than the sh*GFP* control plasmid. The reduction in cellular processes in our study may have contributed to cells appearing more highly oriented. One reason we could not detect a more obvious change in cell orientation with *WNT11* knockdown is that proximal maxillary cells are naturally very oriented. This trend was observed in all specimens analyzed in the study. Thus, it was probably difficult to measure a further increase in alignment above background in the sh*WNT11* knockdown cells. Our results differ from those conducted on the dermomyotome. In two studies, the knockdown of *WNT11* leads to disorganization of myofibers (49, 72). Thus, it is likely that WNT11 has context-dependent functions.

JNK-PCP but Not β-Catenin-mediated WNT Signaling Regulates Cell Migration and Orientation—Based on the data obtained, we suggest that two different WNT pathways, the PCP signaling pathway and the β-catenin-mediated pathway, have distinct effects on the craniofacial mesenchyme. Importantly, our extensive biochemical experiments using luciferase reporters showed that these WNTs trigger different signaling pathways and that WNT11 operates via the DEP domain of DVL. Moving into the *in vivo* condition, only when molecular signaling is directed toward the JNK pathway by exogenous Wnt11, the cells actively migrate. Maxillary cells were also randomized by the ectopic Wnt11. Wnt3a neither attracts nor repels cells. Although we have not directly demonstrated that Wnt3a is required for cell orientation, the effects of exogenous Wnt3a are similar to the control cell line suggesting that β-catenin signaling is not involved in cell orientation.

We can envisage that our findings may extend to other WNTs that do not act via β-catenin. In particular, WNT5A and WNT5B are prominently expressed in the faces of mouse and chicken (35, 81). We showed that RCAS::*WNT5A* injected into the mandibular prominence leads to beak deviations (70). These defects may be due to abnormal cell behavior, which is a question that will be investigated in a separate study. In the mouse, Wnt5a regulates morphogenesis of the secondary palate (32). Cell migration in the palatal shelves was inhibited by loss of *Wnt5a*, as shown in dye injection experiments. Because palatal extension is partially due to elongation and rearrangement of cells (possibly stacking) (14), there is a likelihood that JNK/PCP signaling could be mediating the effects of Wnt5a deficiency.

The cellular and molecular properties of *WNT11* identified here first in the avian face may apply to other WNTs and more generally to other signaling systems. From a technical point of view, the ability to study cell behavior in the dense mesenchyme of a living embryo in a relatively noninvasive manner is a major advance. The next step will be to visualize the subcellular components of the PCP pathway in the presence of different signaling molecules. Finally, our studies on WNT/PCP signaling provide new insights into the pathophysiology of human craniofacial abnormalities such as cleft lip with or without cleft palate.

Acknowledgments—We thank Christoph Niehrs for providing the ATF2 reporter; Claudio Stern and Peter Farlie for providing the DVL mutant constructs; Andrea Münsterberg for providing Wnt3a and Wnt5a cell lines, and Cheng-Ming Fan for generously providing the Wnt11-expressing cell lines.

REFERENCES

1. Minoux, M., and Rijli, F. M. (2010) Molecular mechanisms of cranial neural crest cell migration and patterning in craniofacial development. *Development* **137,** 2605–2621
2. Couly, G. F., Coltey, P. M., and Le Douarin, N. M. (1993) The triple origin of skull in higher vertebrates: a study in quail-chick chimeras. *Development* **117,** 409–429
3. Noden, D. M. (1978) The control of avian cephalic neural crest cytodifferentiation. I. Skeletal and connective tissues. *Dev. Biol.* **67,** 296–312
4. Szabo-Rogers, H. L., Smithers, L. E., Yakob, W., and Liu, K. J. (2010) New directions in craniofacial morphogenesis. *Dev. Biol.* **341,** 84–94
5. Dixon, M. J., Marazita, M. L., Beaty, T. H., and Murray, J. C. (2011) Cleft lip and palate: understanding genetic and environmental influences. *Nat. Rev.*

Genet. **12,** 167–178
6. Bailey, L. J., Minkoff, R., and Koch, W. E. (1988) Relative growth rates of maxillary mesenchyme in the chick embryo. *J. Craniofac. Genet. Dev. Biol.* **8,** 167–177
7. McGonnell, I. M., Clarke, J. D., and Tickle, C. (1998) Fate map of the developing chick face: analysis of expansion of facial primordia and establishment of the primary palate. *Dev. Dyn.* **212,** 102–118
8. Minkoff, R., and Kuntz, A. J. (1977) Cell proliferation during morphogenetic change; analysis of frontonasal morphogenesis in the chick embryo employing DNA labeling indices. *J. Embryol. Exp. Morphol.* **40,** 101–113
9. Minkoff, R., and Kuntz, A. J. (1978) Cell proliferation and cell density of mesenchyme in the maxillary process and adjacent regions during facial development in the chick embryo. *J. Embryol. Exp. Morphol.* **46,** 65–74
10. Patterson, S. B., and Minkoff, R. (1985) Morphometric and autoradiographic analysis of frontonasal development in the chick embryo. *Anatomical Record* **212,** 90–99
11. Szabo-Rogers, H. L., Geetha-Loganathan, P., Nimmagadda, S., Fu, K. K., and Richman, J. M. (2008) FGF signals from the nasal pit are necessary for normal facial morphogenesis. *Dev. Biol.* **318,** 289–302
12. Wu, P., Jiang, T. X., Shen, J. Y., Widelitz, R. B., and Chuong, C. M. (2006) Morphoregulation of avian beaks: comparative mapping of growth zone activities and morphological evolution. *Dev. Dyn.* **235,** 1400–1412
13. Marcucio, R. S., Young, N. M., Hu, D., and Hallgrimsson, B. (2011) Mechanisms that underlie co-variation of the brain and face. *Genesis* **49,** 177–189
14. Economou, A. D., Brock, L. J., Cobourne, M. T., and Green, J. B. (2013) Whole population cell analysis of a landmark-rich mammalian epithelium reveals multiple elongation mechanisms. *Development* **140,** 4740–4750
15. Rodriguez-Boulan, E., and Macara, I. G. (2014) Organization and execution of the epithelial polarity programme. *Nat. Rev.* **15,** 225–242
16. Seifert, J. R., and Mlodzik, M. (2007) Frizzled/PCP signalling: a conserved mechanism regulating cell polarity and directed motility. *Nat. Rev. Genet.* **8,** 126–138
17. Heisenberg, C. P., Tada, M., Rauch, G. J., Saúde, L., Concha, M. L., Geisler, R., Stemple, D. L., Smith, J. C., and Wilson, S. W. (2000) Silberblick/Wnt11 mediates convergent extension movements during zebrafish gastrulation. *Nature* **405,** 76–81
18. Yamaguchi, T. P., Bradley, A., McMahon, A. P., and Jones, S. (1999) A Wnt5a pathway underlies outgrowth of multiple structures in the vertebrate embryo. *Development* **126,** 1211–1223
19. Gao, B., Song, H., Bishop, K., Elliot, G., Garrett, L., English, M. A., Andre, P., Robinson, J., Sood, R., Minami, Y., Economides, A. N., and Yang, Y. (2011) Wnt signaling gradients establish planar cell polarity by inducing Vangl2 phosphorylation through Ror2. *Dev. Cell* **20,** 163–176
20. Rothbächer, U., Laurent, M. N., Deardorff, M. A., Klein, P. S., Cho, K. W., and Fraser, S. E. (2000) Dishevelled phosphorylation, subcellular localization, and multimerization regulate its role in early embryogenesis. *EMBO J.* **19,** 1010–1022
21. Wallingford, J. B., Rowning, B. A., Vogeli, K. M., Rothbächer, U., Fraser, S. E., and Harland, R. M. (2000) Dishevelled controls cell polarity during *Xenopus* gastrulation. *Nature* **405,** 81–85
22. Boutros, M., Paricio, N., Strutt, D. I., and Mlodzik, M. (1998) Dishevelled activates JNK and discriminates between JNK pathways in planar polarity and wingless signaling. *Cell* **94,** 109–118
23. Gao, B. (2012) Wnt regulation of planar cell polarity (PCP). *Curr. Top. Dev. Biol.* **101,** 263–295
24. Kestler, H. A., and Kühl, M. (2008) From individual Wnt pathways towards a Wnt signalling network. *Philos. Trans. R. Soc. Lond. B Biol. Sci.* **363,** 1333–1347
25. Sugimura, R., and Li, L. (2010) Noncanonical Wnt signaling in vertebrate development, stem cells, and diseases. *Birth Defects Res. C Embryo Today* **90,** 243–256
26. Kohn, A. D., and Moon, R. T. (2005) Wnt and calcium signaling: β-catenin-independent pathways. *Cell Calcium* **38,** 439–446
27. Ho, H. Y., Susman, M. W., Bikoff, J. B., Ryu, Y. K., Jonas, A. M., Hu, L., Kuruvilla, R., and Greenberg, M. E. (2012) Wnt5a-Ror-Dishevelled signaling constitutes a core developmental pathway that controls tissue morphogenesis. *Proc. Natl. Acad. Sci. U.S.A.* **109,** 4044–4051
28. Person, A. D., Beiraghi, S., Sieben, C. M., Hermanson, S., Neumann, A. N., Robu, M. E., Schleiffarth, J. R., Billington, C. J., Jr., van Bokhoven, H., Hoogeboom, J. M., Mazzeu, J. F., Petryk, A., Schimmenti, L. A., Brunner, H. G., Ekker, S. C., and Lohr, J. L. (2010) WNT5A mutations in patients with autosomal dominant Robinow syndrome. *Dev. Dyn.* **239,** 327–337
29. Afzal, A. R., Rajab, A., Fenske, C. D., Oldridge, M., Elanko, N., Ternes-Pereira, E., Tüysüz, B., Murday, V. A., Patton, M. A., Wilkie, A. O., and Jeffery, S. (2000) Recessive Robinow syndrome, allelic to dominant brachydactyly type B, is caused by mutation of ROR2. *Nat. Genet.* **25,** 419–422
30. van Bokhoven, H., Celli, J., Kayserili, H., van Beusekom, E., Balci, S., Brussel, W., Skovby, F., Kerr, B., Percin, E. F., Akarsu, N., and Brunner, H. G. (2000) Mutation of the gene encoding the ROR2 tyrosine kinase causes autosomal recessive Robinow syndrome. *Nat. Genet.* **25,** 423–426
31. Gros, J., Hu, J. K., Vinegoni, C., Feruglio, P. F., Weissleder, R., and Tabin, C. J. (2010) WNT5A/JNK and FGF/MAPK pathways regulate the cellular events shaping the vertebrate limb bud. *Curr. Biol.* **20,** 1993–2002
32. He, F., Xiong, W., Yu, X., Espinoza-Lewis, R., Liu, C., Gu, S., Nishita, M., Suzuki, K., Yamada, G., Minami, Y., and Chen, Y. (2008) Wnt5a regulates directional cell migration and cell proliferation via Ror2-mediated noncanonical pathway in mammalian palate development. *Development* **135,** 3871–3879
33. Wyngaarden, L. A., Vogeli, K. M., Ciruna, B. G., Wells, M., Hadjantonakis, A. K., and Hopyan, S. (2010) Oriented cell motility and division underlie early limb bud morphogenesis. *Development* **137,** 2551–2558
34. Geetha-Loganathan, P., Nimmagadda, S., Hafez, I., Fu, K., Cullis, P. R., and Richman, J. M. (2011) Development of high-concentration lipoplexes for in vivo gene function studies in vertebrate embryos. *Dev. Dyn.* **240,** 2108–2119
35. Geetha-Loganathan, P., Nimmagadda, S., Antoni, L., Fu, K., Whiting, C. J., Francis-West, P., and Richman, J. M. (2009) Expression of WNT signalling pathway genes during chicken craniofacial development. *Dev. Dyn.* **238,** 1150–1165
36. Uysal-Onganer, P., and Kypta, R. M. (2012) Wnt11 in 2011, the regulation and function of a non-canonical Wnt. *Acta Physiol.* **204,** 52–64
37. Majumdar, A., Vainio, S., Kispert, A., McMahon, J., and McMahon, A. P. (2003) Wnt11 and Ret/Gdnf pathways cooperate in regulating ureteric branching during metanephric kidney development. *Development* **130,** 3175–3185
38. Nagy, A. (2000) Cre recombinase: the universal reagent for genome tailoring. *Genesis* **26,** 99–109
39. Nagy, A., Moens, C., Ivanyi, E., Pawling, J., Gertsenstein, M., Hadjantonakis, A. K., Pirity, M., and Rossant, J. (1998) Dissecting the role of N-myc in development using a single targeting vector to generate a series of alleles. *Curr. Biol.* **8,** 661–664
40. Lee, J. M., Kim, J. Y., Cho, K. W., Lee, M. J., Cho, S. W., Kwak, S., Cai, J., and Jung, H. S. (2008) Wnt11/Fgfr1b cross-talk modulates the fate of cells in palate development. *Dev. Biol.* **314,** 341–350
41. Chiquet, B. T., Blanton, S. H., Burt, A., Ma, D., Stal, S., Mulliken, J. B., and Hecht, J. T. (2008) Variation in WNT genes is associated with non-syndromic cleft lip with or without cleft palate. *Hum. Mol. Genet.* **17,** 2212–2218
42. Menezes, R., Letra, A., Kim, A. H., Küchler, E. C., Day, A., Tannure, P. N., Gomes da Motta, L., Paiva, K. B., Granjeiro, J. M., and Vieira, A. R. (2010) Studies with Wnt genes and nonsyndromic cleft lip and palate. *Birth Defects Res. A. Clin Mol. Teratol.* **88,** 995–1000
43. Hamburger, V., and Hamilton, H. L. (1951) A series of normal stages in the development of the chick embryo. *J. Morphol.* **88,** 49–92
44. Anakwe, K., Robson, L., Hadley, J., Buxton, P., Church, V., Allen, S., Hartmann, C., Harfe, B., Nohno, T., Brown, A. M., Evans, D. J., and Francis-West, P. (2003) Wnt signalling regulates myogenic differentiation in the developing avian wing. *Development* **130,** 3503–3514
45. Logan, C., and Francis-West, P. (2008) in *Methods in Molecular Biology: Molecular Embryology: Methods and Protocols* (Sharpe, P., Mason, I., and Totowa, N. J., eds) pp. 363–376, Humana Press Inc., Totowa, NJ
46. Lee, S. H., Bédard, O., Buchtová, M., Fu, K., and Richman, J. M. (2004) A new origin for the maxillary jaw. *Dev. Biol.* **276,** 207–224
47. Higashihori, N., Buchtová, M., and Richman, J. M. (2010) The function

and regulation of TBX22 in avian frontonasal morphogenesis. *Dev. Dyn.* **239,** 458–473
48. Plant, M. R., MacDonald, M. E., Grad, L. I., Ritchie, S. J., and Richman, J. M. (2000) Locally released retinoic acid repatterns the first branchial arch cartilages *in vivo*. *Dev. Biol.* **222,** 12–26
49. Gros, J., Serralbo, O., and Marcelle, C. (2009) WNT11 acts as a directional cue to organize the elongation of early muscle fibres. *Nature* **457,** 589–593
50. Das, R. M., Van Hateren, N. J., Howell, G. R., Farrell, E. R., Bangs, F. K., Porteous, V. C., Manning, E. M., McGrew, M. J., Ohyama, K., Sacco, M. A., Halley, P. A., Sang, H. M., Storey, K. G., Placzek, M., Tickle, C., Nair, V. K., and Wilson, S. A. (2006) A robust system for RNA interference in the chicken using a modified microRNA operon. *Dev. Biol.* **294,** 554–563
51. Sharpe, J., Ahlgren, U., Perry, P., Hill, B., Ross, A., Hecksher-Sørensen, J., Baldock, R., and Davidson, D. (2002) Optical projection tomography as a tool for 3D microscopy and gene expression studies. *Science* **296,** 541–545
52. Richman, J. M., and Crosby, Z. (1990) Differential growth of facial primordia in chick embryos: responses of facial mesenchyme to basic fibroblast growth factor (bFGF) and serum in micromass culture. *Development* **109,** 341–348
53. Shimizu, H., Julius, M. A., Giarré, M., Zheng, Z., Brown, A. M., and Kitajewski, J. (1997) Transformation by Wnt family proteins correlates with regulation of β-catenin. *Cell Growth Differ.* **8,** 1349–1358
54. Ishitani, T., Kishida, S., Hyodo-Miura, J., Ueno, N., Yasuda, J., Waterman, M., Shibuya, H., Moon, R. T., Ninomiya-Tsuji, J., and Matsumoto, K. (2003) The TAK1-NLK mitogen-activated protein kinase cascade functions in the Wnt-5a/Ca^{2+} pathway to antagonize Wnt/β-catenin signaling. *Mol. Cell. Biol.* **23,** 131–139
55. Ohkawara, B., and Niehrs, C. (2011) An ATF2-based luciferase reporter to monitor non-canonical Wnt signaling in *Xenopus* embryos. *Dev. Dyn.* **240,** 188–194
56. Voiculescu, O., Bertocchini, F., Wolpert, L., Keller, R. E., and Stern, C. D. (2007) The amniote primitive streak is defined by epithelial cell intercalation before gastrulation. *Nature* **449,** 1049–1052
57. Bookout, A. L., and Mangelsdorf, D. J. (2003) Quantitative real-time PCR protocol for analysis of nuclear receptor signaling pathways. *Nucl. Recept. Signal.* **1,** e012
58. van den Boogaard, M. J., Dorland, M., Beemer, F. A., and van Amstel, H. K. (2000) MSX1 mutation is associated with orofacial clefting and tooth agenesis in humans. *Nat. Genet.* **24,** 342–343
59. Braybrook, C., Doudney, K., Marçano, A. C., Arnason, A., Bjornsson, A., Patton, M. A., Goodfellow, P. J., Moore, G. E., and Stanier, P. (2001) The T-box transcription factor gene TBX22 is mutated in X-linked cleft palate and ankyloglossia. *Nat. Genet.* **29,** 179–183
60. Pauws, E., Hoshino, A., Bentley, L., Prajapati, S., Keller, C., Hammond, P., Martinez-Barbera, J. P., Moore, G. E., and Stanier, P. (2009) Tbx22 null mice have a submucous cleft palate due to reduced palatal bone formation and also display ankyloglossia and choanal atresia phenotypes. *Hum. Mol. Genet.* **18,** 4171–4179
61. Jagomägi, T., Nikopensius, T., Krjutskov, K., Tammekivi, V., Viltrop, T., Saag, M., and Metspalu, A. (2010) MTHFR and MSX1 contribute to the risk of nonsyndromic cleft lip/palate. *Eur. J. Oral Sci.* **118,** 213–220
62. Liang, J., Zhu, L., Meng, L., Chen, D., and Bian, Z. (2012) Novel nonsense mutation in MSX1 causes tooth agenesis with cleft lip in a Chinese family. *Eur. J. Oral. Sci.* **120,** 278–282
63. Salahshourifar, I., Halim, A. S., Wan Sulaiman, W. A., and Zilfalil, B. A. (2011) Contribution of MSX1 variants to the risk of non-syndromic cleft lip and palate in a Malay population. *J. Hum. Genet.* **56,** 755–758
64. Mangold, E., Ludwig, K. U., and Nöthen, M. M. (2011) Breakthroughs in the genetics of orofacial clefting. *Trends Mol. Med.* **17,** 725–733
65. Kondo, S., Schutte, B. C., Richardson, R. J., Bjork, B. C., Knight, A. S., Watanabe, Y., Howard, E., de Lima, R. L., Daack-Hirsch, S., Sander, A., McDonald-McGinn, D. M., Zackai, E. H., Lammer, E. J., Aylsworth, A. S., Ardinger, H. H., Lidral, A. C., Pober, B. R., Moreno, L., Arcos-Burgos, M., Valencia, C., Houdayer, C., Bahuau, M., Moretti-Ferreira, D., Richieri-Costa, A., Dixon, M. J., and Murray, J. C. (2002) Mutations in IRF6 cause Van der Woude and popliteal pterygium syndromes. *Nat. Genet.* **32,** 285–289
66. Li, H., Marijanovic, I., Kronenberg, M. S., Erceg, I., Stover, M. L., Velonis, D., Mina, M., Heinrich, J. G., Harris, S. E., Upholt, W. B., Kalajzic, I., and Lichtler, A. C. (2008) Expression and function of Dlx genes in the osteoblast lineage. *Dev. Biol.* **316,** 458–470
67. Tadic, T., Dodig, M., Erceg, I., Marijanovic, I., Mina, M., Kalajzic, Z., Velonis, D., Kronenberg, M. S., Kosher, R. A., Ferrari, D., and Lichtler, A. C. (2002) Overexpression of Dlx5 in chicken calvarial cells accelerates osteoblastic differentiation. *J. Bone Miner. Res.* **17,** 1008–1014
68. Satokata, I., Ma, L., Ohshima, H., Bei, M., Woo, I., Nishizawa, K., Maeda, T., Takano, Y., Uchiyama, M., Heaney, S., Peters, H., Tang, Z., Maxson, R., and Maas, R. (2000) Msx2 deficiency in mice causes pleiotropic defects in bone growth and ectodermal organ formation. *Nat. Genet.* **24,** 391–395
69. Wilkie, A. O., Tang, Z., Elanko, N., Walsh, S., Twigg, S. R., Hurst, J. A., Wall, S. A., Chrzanowska, K. H., and Maxson, R. E., Jr. (2000) Functional haploinsufficiency of the human homeobox gene MSX2 causes defects in skull ossification. *Nat. Genet.* **24,** 387–390
70. Hosseini-Farahabadi, S., Geetha-Loganathan, P., Fu, K., Nimmagadda, S., Yang, H. J., and Richman, J. M. (2013) Dual functions for WNT5A during cartilage development and in disease. *Matrix Biol.* **32,** 252–264
71. Gao, C., and Chen, Y. G. (2010) Dishevelled: The hub of Wnt signaling. *Cell. Signal.* **22,** 717–727
72. Morosan-Puopolo, G., Balakrishnan-Renuka, A., Yusuf, F., Chen, J., Dai, F., Zoidl, G., Lüdtke, T. H., Kispert, A., Theiss, C., Abdelsabour-Khalaf, M., and Brand-Saberi, B. (2014) Wnt11 is required for oriented migration of dermogenic progenitor cells from the dorsomedial lip of the avian dermomyotome. *PLoS One* **9,** e92679
73. Diewert, V. M., and Lozanoff, S. (1993) Growth and morphogenesis of the human embryonic midface during primary palate formation analyzed in frontal sections. *J. Craniofac. Genet. Dev. Biol.* **13,** 162–183
74. Diewert, V. M., and Wang, K. Y. (1992) Recent advances in primary palate and midface morphogenesis research. *Crit. Rev. Oral Biol. Med.* **4,** 111–130
75. Jiang, R., Bush, J. O., and Lidral, A. C. (2006) Development of the upper lip: morphogenetic and molecular mechanisms. *Dev. Dyn.* **235,** 1152–1166
76. Wang, K. Y., Juriloff, D. M., and Diewert, V. M. (1995) Deficient and delayed primary palatal fusion and mesenchymal bridge formation in cleft lip-liable strains of mice. *J. Craniofac. Genet. Dev. Biol.* **15,** 99–116
77. Ashique, A. M., Fu, K., and Richman, J. M. (2002) Endogenous bone morphogenetic proteins regulate outgrowth and epithelial survival during avian lip fusion. *Development* **129,** 4647–4660
78. Abramyan, J., Leung, K. J., and Richman, J. M. (2014) Divergent palate morphology in turtles and birds correlates with differences in proliferation and BMP2 expression during embryonic development. *J. Exp. Zool. B Mol. Dev. Evol.* **322,** 73–85
79. Li, X., Young, N. M., Tropp, S., Hu, D., Xu, Y., Hallgrímsson, B., and Marcucio, R. S. (2013) Quantification of shape and cell polarity reveals a novel mechanism underlying malformations resulting from related FGF mutations during facial morphogenesis. *Hum. Mol. Genet.* **22,** 5160–5172
80. Perrimon, N., Pitsouli, C., and Shilo, B. Z. (2012) Signaling mechanisms controlling cell fate and embryonic patterning. *Cold Spring Harbor Perspect. Biol.* **4,** a005975
81. Summerhurst, K., Stark, M., Sharpe, J., Davidson, D., and Murphy, P. (2008) 3D representation of Wnt and Frizzled gene expression patterns in the mouse embryo at embryonic day 11.5 (Ts19). *Gene. Expr. Patterns* **8,** 331–348
82. Chen, A. E., Ginty, D. D., and Fan, C. M. (2005) Protein kinase A signalling via CREB controls myogenesis induced by Wnt proteins. *Nature* **433,** 317–322